Geophysical Research Letters

RESEARCH LETTER
10.1029/2023GL107360

A Tilted Broad Plume Underneath the Greenland Cratonic Keels

Dan Wang[1,2,3], **Stephen S. Gao**[2], **Yangyang Liao**[2], **and Kelly H. Liu**[2]

[1]College of Environment and Civil Engineering, Chengdu University of Technology, Chengdu, China, [2]Geology and Geophysics Program, Missouri University of Science and Technology, Rolla, MO, USA, [3]Earthquake Research Center, Chengdu University of Technology, Chengdu, China

Key Points:

- The central and east Greenland shows abnormal mantle transition zone (MTZ) thickness, indicating a deep-seated mantle plume
- Seismic data unveil the impact of post-garnet phase transition at the 660-km discontinuity on mantle dynamics
- Variations in MTZ thickness suggest the existence of a tilted plume and offer insights into the plume behavior

Supporting Information:

Supporting Information may be found in the online version of this article.

Correspondence to:

K. H. Liu,
liukh@mst.edu

Citation:

Wang, D., Gao, S. S., Liao, Y., & Liu, K. H. (2024). A tilted broad plume underneath the Greenland cratonic keels. *Geophysical Research Letters*, *51*, e2023GL107360. https://doi.org/10.1029/2023GL107360

Received 17 NOV 2023
Accepted 4 APR 2024

Author Contributions:

Conceptualization: Stephen S. Gao, Kelly H. Liu
Data curation: Dan Wang
Formal analysis: Dan Wang, Yangyang Liao
Funding acquisition: Stephen S. Gao, Kelly H. Liu
Investigation: Dan Wang
Methodology: Stephen S. Gao, Kelly H. Liu
Project administration: Kelly H. Liu
Resources: Kelly H. Liu
Software: Stephen S. Gao, Kelly H. Liu
Supervision: Kelly H. Liu
Validation: Stephen S. Gao, Kelly H. Liu
Visualization: Yangyang Liao
Writing – original draft: Dan Wang

Abstract To advance our comprehension of the complex geological history and mantle dynamics in the North Atlantic region, we employ all available broadband seismic data recorded in Greenland to reveal an abnormal mantle transition zone (MTZ) structure. Central and eastern Greenland exhibits depressed 410 and 660 km discontinuities (d410 and d660, respectively) bordering the MTZ, indicative of a substantial thermal anomaly associated with an underlying plume, surpassing the 1,800°C threshold for post-garnet phase transitions at the d660. Variations in MTZ thickness across Greenland stem from differing temperature anomalies at the d410 and d660, possibly linked to a tilted plume within the MTZ. These findings corroborate geodynamic models, elucidating the interaction between post-garnet phase transitions and upwelling plumes. The results shed light on the origin of the enigmatic Icelandic hotspot track and its influence on the thermal and lithospheric structures beneath Greenland.

Plain Language Summary The physical and chemical processes responsible for producing the magnificent volcanic eruptions in Iceland and the North Atlantic region are debated issues in the geoscientific community despite numerous field and laboratory studies over the past several decades. One of the hypotheses for the formation of the volcanoes is that they originate from a column of hot rocks rising from the deep mantle, that is, a mantle plume. The geometry, depth extent, and temperature anomaly of the plume are not well defined but can be constrained using the topography of two phase-transition boundaries approximately at the globally averaged depths of 410 and 660 km, respectively. By analyzing *P*-to-*S* converted phases from the two discontinuities recorded by seismic stations, our results support the existence of a mantle plume that is broader than most other plumes on Earth beneath east Greenland. In addition, the results suggest that the nature of the phase transition across the 660 km discontinuity is different between the hottest core of the plume stem and the colder peripheral areas. The existence of the particular type of phase transition in the plume center can explain the large dimension of the plume, the excessive volcanism and other observations in the area.

1. Introduction

The Greenland continent has a long and complex tectonic history since its origin as part of the Laurentian core underlain by a Precambrian continental shield comprising an Archean craton and several Paleoproterozoic orogenic belts (Darbyshire et al., 2018). Geologists and seismologists identified three major orogens along the margins of Greenland (Grocott & McCaffrey, 2017), including the Ketilidian Orogenic Belt, the Nagssugtoqidian Orogenic Belt, and the East Caledonian Orogenic Belt, along with the three cratonic keels, the Rae Craton, the North Atlantic Craton, and the Inglefield-Melville Craton, characterized by the separated bodies of strong high-velocity anomalies in the upper mantle (Figure 1; Celli et al., 2021). The opening of the Atlantic Ocean led to a separation of Greenland and North America at ~125 Ma (Buiter & Torsvik, 2014). Then, the Labrador Sea and the Baffin Bay opened from south to north (Peace et al., 2017) as the seafloor spreading of the Atlantic Ocean occurred between ~61 and 79 Ma until ~35–33 Ma (Chalmers, 1991; Roest & Srivastava, 1989), which produced the substantial volcanisms on the west and east Greenland coasts (Figure 1; Wilkinson et al., 2017). During this period, the extensive rework of the Greenland mantle by the impingement of the Iceland plume as Greenland drifted west induced a wide sequence of magmatic activity across the North Atlantic region (Darbyshire et al., 2018).

An increasing number of seismic tomography studies aimed at providing a detailed structure of the Greenland mantle and crust have been conducted in the past several years (e.g., Antonijevic & Lees, 2018; Mordret, 2018;

Writing – review & editing: Dan Wang, Stephen S. Gao, Yangyang Liao, Kelly H. Liu

Pourpoint et al., 2018; Toyokuni & Zhao, 2021; Toyokuni et al., 2020). The common feature revealed by most of these tomography studies is an elongated zone with lower-velocity anomalies and a relatively thin lithosphere spanning from the west to the east coasts of central Greenland, even though its direction and spatial and depth extents are debated (Celli et al., 2021; Lebedev et al., 2018; Mordret, 2018; Rickers et al., 2013; Toyokuni & Zhao, 2021; Toyokuni et al., 2020). This elongated zone has been proposed to be associated with the trajectory of the Iceland hotspot as the Greenland continent drifted over a mantle plume (Lebedev et al., 2018; Mordret, 2018; Pourpoint et al., 2018; Rickers et al., 2013; Toyokuni et al., 2020). However, the location of the Iceland hotspot track is not well constrained and spreads over a large area, presenting large uncertainties in the proposed tracks and probably indicating a complex thermal structure underneath the Greenland continent (Figure 1). Particularly, a recent regional tomography study by Celli et al. (2021) reveals a tilted plume tail originating from the mantle transition zone (MTZ) beneath the east coast of Greenland that gets deflected by the thick cratonic keel and flows obliquely in the upper mantle toward Iceland, which highlights the complexity of the plume and mantle structure beneath the North Atlantic region.

The MTZ between the upper and lower mantle is bounded by two sharp interfaces of seismic wave speeds: the 410 km discontinuity (d410) and the 660 km discontinuity (d660). The d410 has a positive Clapeyron slope (Bina & Helffrich, 1994) ranging from 1.5 to 5.0 MPa/K (see a review by Faccenda & Dal Zilio, 2017) and represents the exothermic transition from olivine to wadsleyite, while the phase transition and the sign of the Clapeyron slope at the d660 are temperature dependent. When the ambient temperature is less than about 1,800°C (Ishii et al., 2018), the phase transition is dominated by the transition from ringwoodite to perovskite (pSp) with a Clapeyron slope ranging from −3.9 to −0.55 MPa/K (Faccenda & Dal Zilio, 2017). However, when mantle temperatures are higher than ∼1,800°C (Ishii et al., 2018), the dominant phase transition at the d660 is from majorite garnet to perovskite (pGt), which, in contrast to the pSp transition, has a positive Clapeyron slope ranging from +0.8 to +6.4 MPa/K (Faccenda & Dal Zilio, 2017). The involvement of the additional phase transition at the d660 leads to more complicated patterns of MTZ thickness variations in areas with a high-temperature MTZ (Deuss, 2007; Jenkins et al., 2016).

The receiver function (RF) technique can provide a detailed topography of the d410 and d660, thus the thermal structure of the MTZ. Using 24 local seismic stations on the east Greenland coast, Kraft et al. (2018) find overall depressed d410 and d660 and propose a positive thermal anomaly associated with the passage of Greenland over the Iceland mantle plume. However, for the whole Greenland continent, there is a lack of a comprehensive examination of MTZ discontinuity structures, probably because of a lack of sufficient coverage by seismic stations. With an increasing number of seismic stations and available data in Greenland and adjacent areas, additional investigations of the MTZ beneath the entire Greenland region can provide insights into plume dynamics and its impacts on the mantle structure in the North Atlantic region. In this study, we image the MTZ structure beneath the entire Greenland continent using a compilation of all the available broadband seismic data sets. This study presents an unprecedentedly comprehensive image of the MTZ structure and provides new insights into the heterogeneous mantle dynamics in the Greenland region.

2. Data and Methods

2.1. Teleseismic Data

We acquired three-component broadband seismic data recorded by 44 stations in Greenland from the former Incorporated Research Institutions for Seismology Data Management Center (now the EarthScope Consortium Seismological Facility for the Advancement of Geoscience or SAGE) for the recording period from 1985 to 2023 (Figure 1). Detailed information about the stations and networks can be found in Table S1 in Supporting Information S1. The distribution of events is shown in the inset map of Figure 1, and the number of RFs per circular bin can be found in Figure S1 in Supporting Information S1. The data requesting and processing procedure used in this study is the same as that used in Gao and Liu (2014a) for an MTZ study in the contiguous United States. In this study, we used an approach that assumes non-plane wave (Gao & Liu, 2014a, 2014b), which takes into consideration the difference in the ray parameters between the direct P-wave and the converted *S*-wave at each discontinuity, leading to more accurately determined discontinuity depths comparing to traditional RF studies under the plane-wave assumption. Detailed data request and processing procedures are summarized in Supporting Information S1.

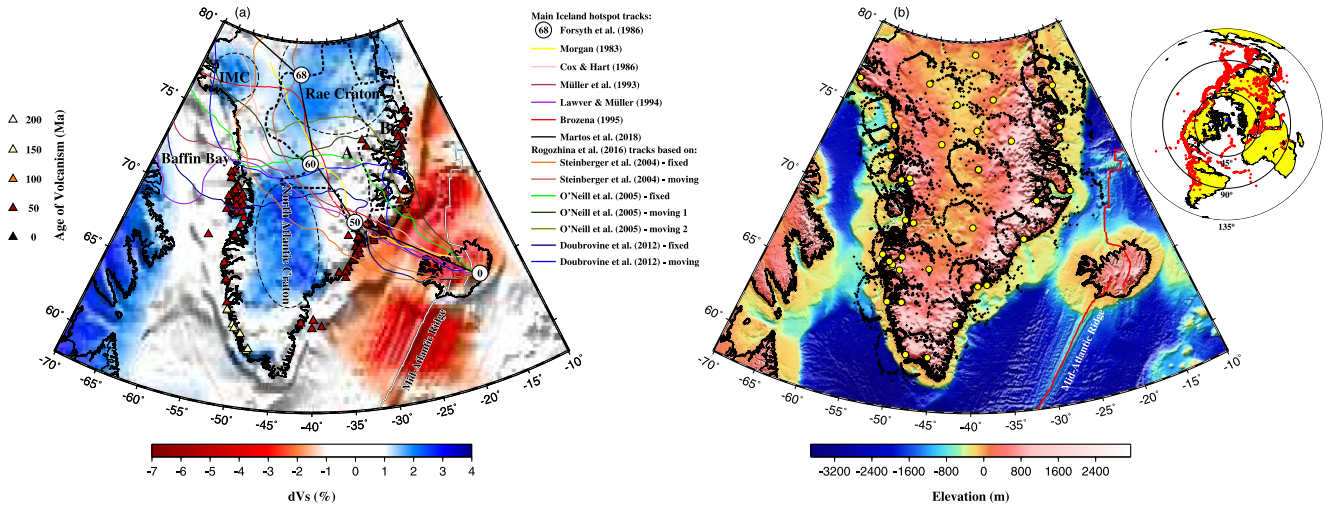

Figure 1. (a) Major tectonic features of the study area plotted on a topographic map with the background color showing the averaged *S* wave velocity anomalies in the upper mantle (from 0 to 410 km) derived from the NAT2021 regional tomography model (Celli et al., 2021). The solid black line is the proposed Iceland hotspot track inferred from a recently published geothermal heat flux study (Martos et al., 2018). The white circles and numbers are the aged positions of the plume track based on Forsyth et al. (1986). The colored solid lines illustrate the possible Icelandic hotspot tracks (Brozena, 1995; A. H. R. B. Cox, 1986; Doubrovine et al., 2012; Forsyth et al., 1986; Morgan, 1983; Müller et al., 1993; O'Neill et al., 2005; Steinberger et al., 2004). Colored triangles are volcanoes in Greenland whose ages were compiled by Wilkinson et al. (2017). The three main craton units illustrated by the black dashed circles and ellipse are from Celli et al. (2021). IMC: Inglefield-Melville Craton. The black dash lines circle the areas A and B, which show abnormal mantle transition zone thickness and discontinuity depths. (b) A topographic relief and bathymetry map of the study area showing seismic stations (yellow dots) was used in this study, as well as the ray-piecing points (black pluses) at 535 km depth. The solid red line represents the mid-Atlantic ridge. The inset at the top right shows the events used in this study.

2.2. Velocity Corrections Using Recent Regional and Global Velocity Models

As elucidated in Supporting Information S1, we applied moveout correction using the one-dimensional IASP91 standard Earth model, which implies that the resulting depths and MTZ thickness are apparent rather than true values. In order to determine the true discontinuity depths, we correct the apparent depths using the approach proposed by Gao and Liu (2014b). The velocity corrections require accurately determined P and S wave velocity models with similar spatial and depth coverage. Among many published velocity models for the study area, in this study, we use some of the most recent ones (Figure S2 in Supporting Information S1), which contain both *P* and *S* velocity information: the regional *S*-wave model NAT2021 (Celli et al., 2021), the regional *P*-wave model Toyokuni2020 (Toyokuni et al., 2020), and the global V_p and V_s model TX2019Slab (Lu et al., 2019), to correct the apparent depths. In order to minimize the bias of the estimated temperature anomalies associated with the different Clapeyron slope estimates, we take the averaged Clapeyron slopes of previously published values discussed in a review article by Faccenda and Dal Zilio (2017): +3.10 MPa/K for the olivine to wadsleyite transition at the d410, and −2.34 MPa/K for the pSp phase transition and +2.72 MPa/K for the pGt phase transition at the d660.

3. Results

3.1. Apparent Discontinuity Depths and MTZ Thickness

As demonstrated in Figure 2 and Figure S3 in Supporting Information S1, robust arrivals corresponding to the d410 and d660 can be unambiguously identified on the vast majority of the resulting depth series. The apparent results, shown in Figures 3a–3c, reveal that the deepest apparent d410 depths are concentrated in the central-eastern part of Greenland (approximately within the longitude range of −38° to −41° along the N73 latitude, Figures S4 and S5 in Supporting Information S1), while the shallowest d410 depths are consistently observed beneath the cratons, corresponding to the lows and highs of the mean dV_p in the upper mantle from the velocity models (Figure 2). In contrast, the d660 results reveal its deepest apparent depths on the east coast of Greenland (specifically around −25° to −27° in longitude along the N71 latitude, Figures S4 and S5 in Supporting Information S1), which is notably east of the region associated with the deepest apparent d410 depths. The shallowest apparent d660 depths are predominantly situated beneath the cratons, exhibiting a distribution similar to that of

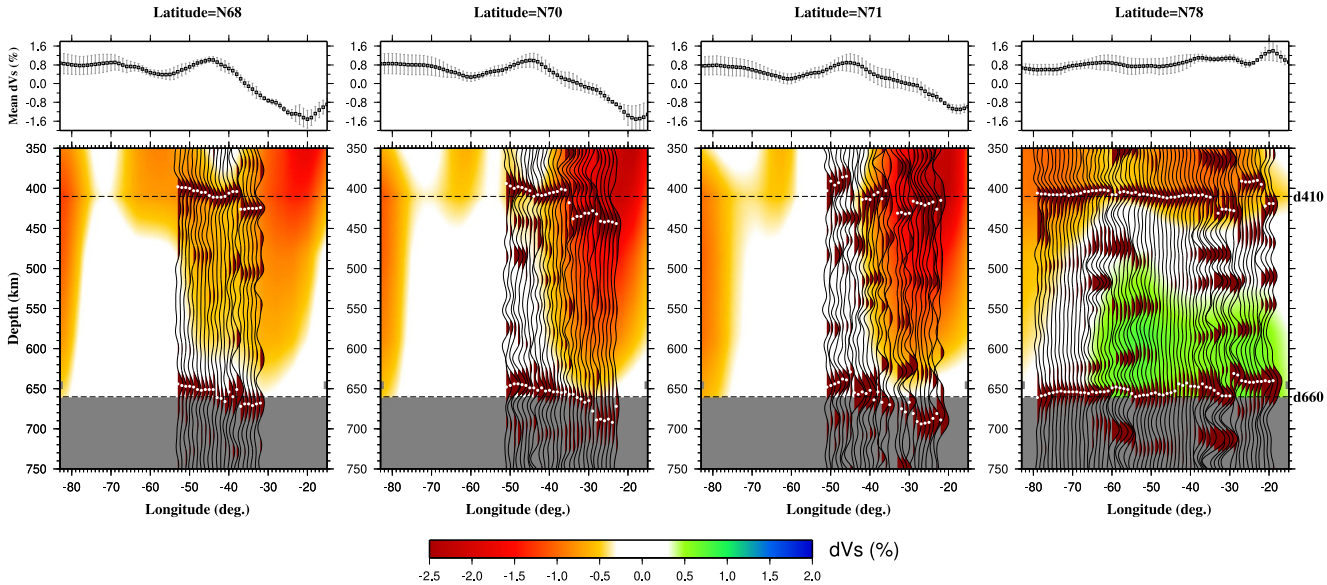

Figure 2. Resulting stacked receiver functions along four latitudinal profiles. The background image shows the V_s anomalies from the NAT2021 Model (Celli et al., 2021), and the white dots on the traces indicate the picked arrivals for the d410 and d660. The latitudes N70 and N71 profiles are cross the plume center, while latitudes 68 and 78 are close to the southern and northern ends of the plume area, respectively. The full 20 latitudinal profiles can be found in Figure S4 in Supporting Information S1. The top panels show the mean averaged dV_s and its associated standard deviations (small bars) for three velocity models as a function of longitudes for each profile.

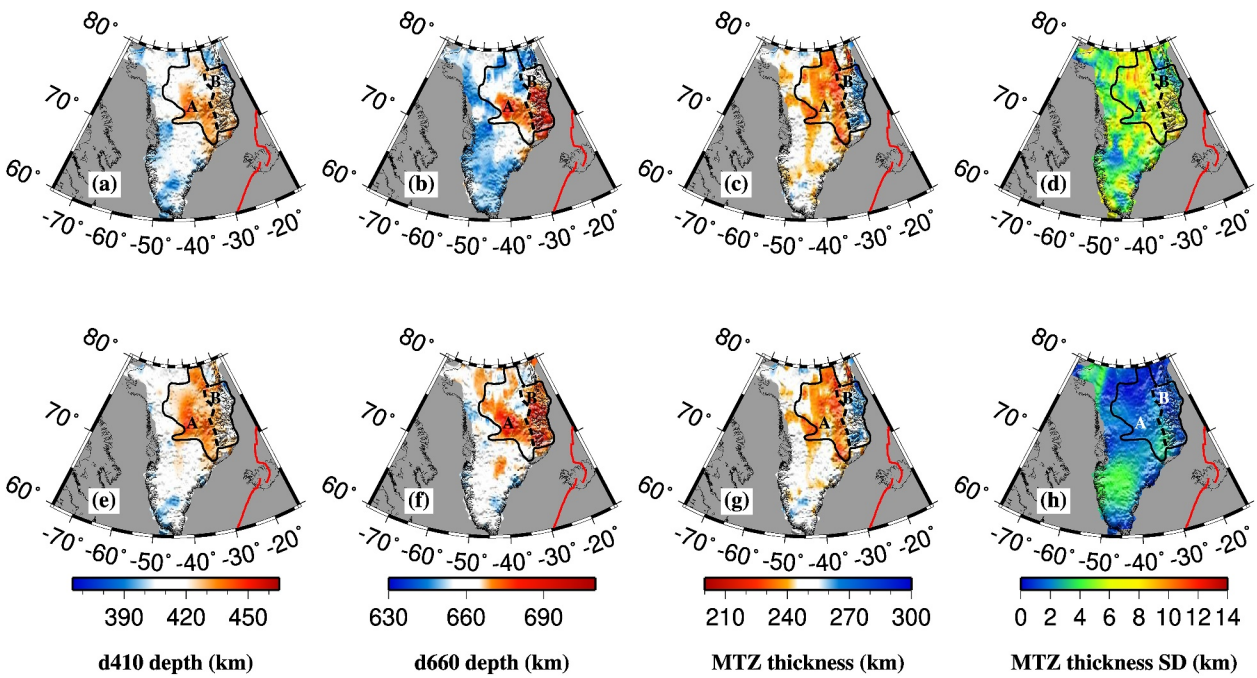

Figure 3. Resulting apparent (a–d) and mean velocity-corrected (e–h) depths of the d410 and d660 and mantle transition zone (MTZ) thickness. (a) Apparent d410 depths. (b) Apparent d660 depths. (c) Apparent MTZ thickness. (d) Standard deviation (SD) of the MTZ thickness. (e) Mean d410 depths corrected by three velocity models. (f) Mean d660 depths corrected by three velocity models. (g) Mean corrected MTZ thickness. (h) SD of the mean corrected MTZ thickness. The black solid line outlines the area with abnormal MTZ thickness characterized by the depression of both discontinuities. The black dashed line separates areas A and B with different MTZ thickness patterns.

the d410 but with broader coverage. Remarkably, the region with the deepest apparent d660 depths on the east coast of Greenland corresponds to a thicker-than-normal MTZ, aligning with the findings of Kraft et al. (2018). Conversely, the central Greenland area to the west of this region is characterized by a thinner-than-normal MTZ.

3.2. Regions With Abnormal MTZ Thickness After Velocity Corrections

Following velocity corrections applied to apparent depths using the velocity models (Figure S2 in Supporting Information S1), small disparities among the corrected results by these models became evident (Figure S6 in Supporting Information S1). To minimize these differences, we utilized the mean corrected results for our interpretations (Figures 3e–3h). Based on the mean corrected results, the majority of the southern part of the Greenland continent exhibits normal discontinuity depths, largely attributed to the removal of the influence of high-velocity anomalies associated with the cratonic keels in the upper mantle and crust. However, in central and eastern Greenland, both the d410 and d660 remain depressed, indicated by the enclosed region of the black solid line in Figure 3, leading to an abnormal MTZ thickness. This persistent depression suggests the presence of an exceptionally high-temperature regime in the MTZ. The average depths, after velocity corrections, for the d410 and d660 are 428.6 ± 12.4 and 672.3 ± 9.0 km, respectively. Both discontinuities are deeper than the global average values of 411 km (Gu et al., 1998) and 654 km (Gu & Dziewonski, 2002) for the d410 and d660, respectively. Within this region, where both the d410 and d660 exhibit depression, there is an observed increase in MTZ thickness from central Greenland (averaging 237.8 ± 9.5 km) to the east coast (averaging 254.2 ± 16 km). The overall average MTZ thickness beneath these two areas is comparable to the global average of 247 km (Tauzin et al., 2008) beneath the hotspots.

The region with varying MTZ thickness and depressions of both discontinuities is divided into two areas: Area A in the central part and Area B on the east coast of Greenland, separated by a dashed line in Figure 3. In Area A, the thinner-than-normal MTZ is primarily attributed to the greater depression of the d410 compared to the d660. The average depths for the d410 and d660 are 432.1 ± 9.1 and 670.0 ± 9.1 km, respectively. Conversely, in Area B on the east coast of Greenland, the MTZ is thicker than normal. The average d660 depth is 676.5 ± 7.3 km, which is deeper than in Area A, and the average d410 depth is 422.3 ± 14.9 km. Therefore, the lateral topographical variations of the MTZ discontinuities contribute to the different MTZ thickness patterns in this region.

4. Discussion

4.1. A Broad Plume With Lateral Temperature Variations

We estimated the temperature anomalies in the vicinity of the MTZ discontinuities using the averaged Clapeyron slopes of previously published values, as mentioned in Section 2.2. Under a hot regime, the depression of the d660 is thought to be caused by the post-garnet phase transition dominating across the d660, which has a positive Clapeyron slope (Deuss, 2007; Jenkins et al., 2016). For the entire region with depressed discontinuities and abnormal MTZ thickness (areas A & B), the estimated temperature anomalies at both the d410 and the d660 are about +210°C and +160°C. Assuming a normal temperature of 1,687°C just below the d660 (Katsura, 2022), the estimated temperature at the d660 is about 1,847°C, which exceeds the proposed temperature of 1,800°C required for the dominance of the post-garnet phase transition (Ishii et al., 2018). Therefore, the simplest model that can explain the depression of the MTZ discontinuities beneath central and east Greenland involves a plume with a broad positive thermal anomaly of approximately 210°C at the d410 and 160°C at the d660, traversing the entire MTZ under the post-garnet phase transition at the d660. The deepening of both the d660 and the d410 can also be observed from other global hotspots within a similar temperature anomaly range based on RFs (Tauzin et al., 2008) and SS precursors (Deuss, 2007), such as Tahiti and Easter hotspots, where the observations are also explained by the post-garnet phase transition at the d660 under a hotter regime than other hotspots with an uplifted d660 (e.g., Samoa hotspot). Furthermore, we also estimated the temperature anomalies for both discontinuities beneath areas A and B. For Area A, the estimated temperature anomaly is higher at the d410 (+250°C) than at the d660 (+133°C). On the other hand, the estimated temperature anomalies are +137°C at the d410 and +213°C at the d660 beneath Area B. Therefore, there is a lateral variation of the temperature at the d410 and the d660, possibly due to the tilted upwelling from Area B toward Area A inside the MTZ. The increasing amplitude of low velocity toward central Greenland in the MTZ can also be seen in a recent tomography study (Celli et al., 2021). This observation confirms the thermal structure of the MTZ is not vertically coherent, as suggested by a recent review study (Goes et al., 2022).

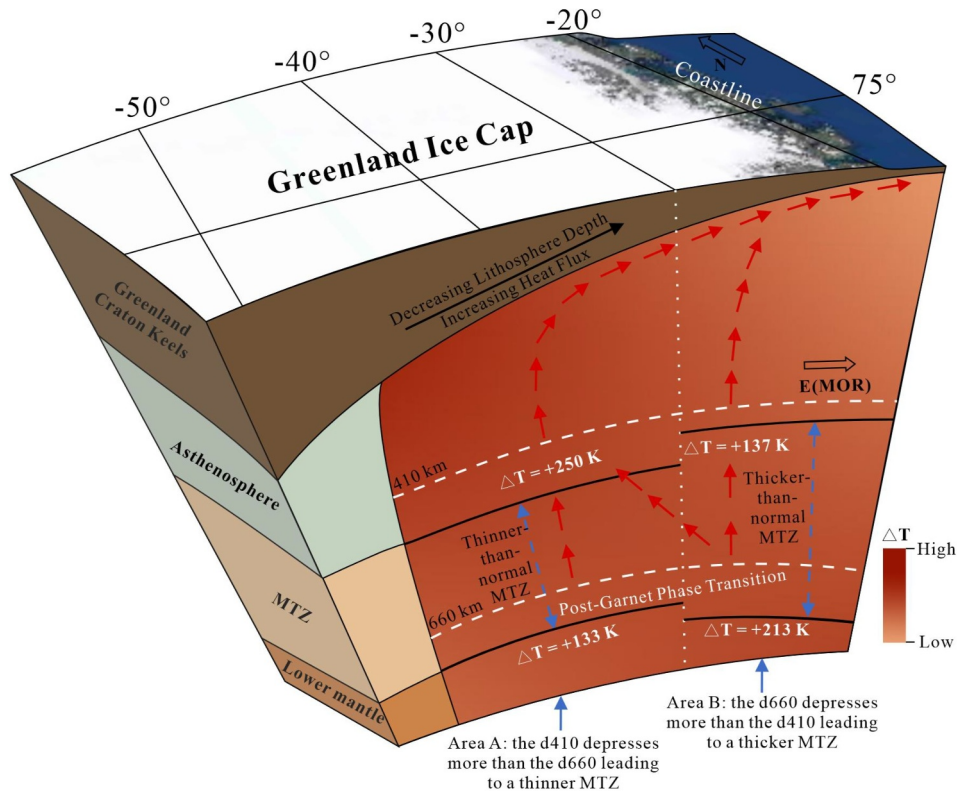

Figure 4. A schematic E-W depiction of the interpreted models showing the major characteristics of the topography of the mantle transition zone (MTZ) discontinuities. The dominant mineral phase transition across the d660 beneath central and east Greenland (areas A & B) is the post-garnet phase transition. The topographic variations of MTZ discontinuities are based on the average discontinuity depths for areas A and B and indicate lateral temperature variations associated with the tilted upwelling, which is indicated by the red arrows. The white vertical dashed line represents the boundary between areas A and B.

4.2. Plume Dynamics

Recent geodynamic modeling studies (Liu et al., 2018) suggest that the involvement of the post-garnet phase transition at the d660 leads to significant enhancements in the size, strength, and volume flux of upwelling plumes compared to mantle plumes dominated by post-spinel phase transition at temperatures lower than the post-garnet transition. These enhancements are primarily attributed to the decomposition of ringwoodite into garnet and magnesiowüstite, resulting in a density drop (Ishii et al., 2018; Liu et al., 2018). Our observations (Figure 3) provide empirical evidence supporting this model. Areas A and B exhibit various geophysical features, including the thinnest lithosphere (Figure S7 in Supporting Information S1), a pronounced low-velocity anomaly in the upper mantle (Figure 1), the highest geothermal heat flux (Figure S7 in Supporting Information S1), and a significant density decrease according to gravity data beneath Greenland (Minakov & Gaina, 2021). These features coincide with the location of the observed high-temperature anomaly at the d660 and may be attributed to increased thermal and heat transfer facilitated by the enhanced upwelling strength and volume flux of the broad plume (Artemieva, 2019; Kumar et al., 2005; Martos et al., 2018; Minakov & Gaina, 2021; Mordret, 2018; Rogozhina et al., 2016). Comparatively, Area B exhibits a shallower lithosphere-asthenosphere boundary and stronger heat flux but a lower estimated temperature at the d410 compared to Area A (Figure S7 in Supporting Information S1). This variation might be explained by the deflection of upwelling in the upper mantle by cratonic keels beneath central Greenland and relatively weak lithosphere toward the Mid-oceanic Ridge (Figure 4), as suggested by several studies (Artemieva & Mooney, 2002; Celli et al., 2021; Sleep, 1997; Sleep et al., 2002). There are several tilted mantle plumes identified by previous geophysical, geodynamic, and geochemical studies, such as the African superplume (Hansen & Nyblade, 2013; Hansen et al., 2012; Moucha & Forte, 2011), the Hawaiin hotspot (Wölbern et al., 2006), the Yellowstone hotspot (Nelson & Grand, 2018; Shervais & Hanan, 2008; Steinberger et al., 2019), and Iceland (Rasmussen et al., 2020; Shen et al., 2002). The tilting can be

caused by mantle flow or mantle-wide convection (mantle wind) (Kerr & Mériaux, 2004; Koppers et al., 2021; Nelson & Grand, 2018; Steinberger et al., 2019), plate motion (Whitehead, 1982), subducting slab (Geist & Richards, 1993; Mériaux et al., 2016), and compositional heterogeneities (Hanan & Schilling, 1997). Compared with these studies, the broad plume we identified in this study is underneath the thick Greenland craton keels and close to the mid-oceanic ridge. Therefore, the westward tilted upwelling in the MTZ may be caused by the mantle wind, which has a comparable direction to the plate motion (R. T. Cox, 1999). On the other hand, the deflected upwelling in the upper mantle may mainly be due to the interaction of the plume and the craton keels, causing variations in mantle density and viscosity.

Furthermore, the wide distribution of the proposed locations of the hotspot track (Figure 1) in the North Atlantic region, including the Greenland continent, could be attributed to the interaction of the broad plume with the lithosphere when Greenland began drifting westward between 90 and 60 Ma (Steinberger et al., 2019). Given that a substantial portion of the previously posited hotspot tracks resides within the expansive plume, the intricate thermal structure beneath Greenland may stem from the interaction of the tilted broad plume with the thick craton lithosphere, in conjunction with the plate motion history. Our model (Figure 4) provides insights into long-standing debates concerning the origin, morphology, widespread volcanism, and the extent of the Icelandic hotspot track in the Greenland region.

5. Conclusions

In this study, we used a comprehensive data set of seismic records to image the MTZ beneath the entire Greenland continent. Our findings reveal intriguing details about the MTZ structure and its implications for the mantle dynamics of the region. The study reveals the presence of abnormal MTZ thickness in central and eastern Greenland, marked by a depression of the d410 and d660, suggesting the existence of the post-garnet phase transition at the d660. Different regions within Greenland exhibit variations in MTZ thickness, with thinner-than-normal MTZ in central Greenland and thicker-than-normal MTZ on the east coast. The variations are linked to differences in the temperature anomaly at the d410 and d660, possibly due to the tilted upwelling of the plume within the MTZ. These variations in MTZ thickness and temperature are consistent with recent geodynamic modeling studies, which suggest that the post-garnet phase transition at the d660 may lead to enhanced upwelling plumes with increased size, strength, and volume flux, resulting in various geophysical features, such as thinner lithosphere, a low-velocity anomaly in the upper mantle, and higher geothermal heat flux. Our findings provide empirical support for the geodynamic model that links post-garnet phase transitions at the d660 with the behavior of upwelling plumes.

Data Availability Statement

All the data used in the study are publicly available from the Seismological Facility for the Advancement of Geoscience Data Management Center (https://www.iris.edu/hq/sage; last accessed: July 2023) under network code 9D (https://doi.org/10.7914/SN/9D_2010; Motyka et al., 2010), DK (http://www.fdsn.org/networks/detail/DK/), G (https://doi.org/10.18715/GEOSCOPE.G), GE (https://doi.org/10.14470/TR560404), GG (https://doi.org/10.7914/SN/GG), IU (https://doi.org/10.7914/SN/IU), KP (https://doi.org/10.7914/SN/KP; Lee & Park, 2013), X3 (https://doi.org/10.7914/SN/X3_2007; Fahnestock & Truffer, 2007), XF (https://doi.org/10.7914/SN/XF_2014; Nettles, 2014), YF (https://doi.org/10.7914/SN/YF_2012; Holland, 2012), YM (https://doi.org/10.7914/SN/YM_2013; Bartholomaus & Catania, 2013), YV (http://www.fdsn.org/networks/detail/YV_2000/), and ZN (http://www.fdsn.org/networks/detail/ZN_2006/). While we used the BREQ_FAST procedure (https://ds.iris.edu/ds/nodes/dmc/forms/breqfast-request/) for data requesting, please be advised that BREQ_-FAST will be retired between June 2024 and the end of the year after 36 years of service, and the same data set can be request by alternatives such as FetchData and ROVER. The specific data requesting parameters, including the cut-off magnitude and epicentral distance range, can be found in Section 2.1 and the Text S1 in Supporting Information S1. Figures were made with Generic Mapping Tools version 4.5.18 (Wessel et al., 2019) and CorelDRAW 2021 (https://www.coreldraw.com/en/).

Acknowledgments
The facilities of SAGE Data Services, and specifically the SAGE Data Management Center, were used for access to waveforms and related metadata used in this study. SAGE Data Services are funded through the Seismological Facilities for the Advancement of Geoscience Award of the National Science Foundation under Cooperative Support Agreement EAR-1851048. We thank Jeffrey Gu, an anonymous reviewer, and Editor Daoyuan Sun for constructive reviews. The study was partially supported by the U.S. National Science Foundation under awards 1830644, 2149587 to K.L., and 1919789 to S.G.

References

Antonijevic, S. K., & Lees, J. M. (2018). Effects of the Iceland plume on Greenland's lithosphere: New insights from ambient noise tomography. *Polar Science*, *17*, 75–82. https://doi.org/10.1016/j.polar.2018.06.004

Artemieva, I. M. (2019). Lithosphere thermal thickness and geothermal heat flux in Greenland from a new thermal isostasy method. *Earth-Science Reviews*, *188*, 469–481. https://doi.org/10.1016/j.earscirev.2018.10.015

Artemieva, I. M., & Mooney, W. D. (2002). On the relations between cratonic lithosphere thickness, plate motions, and basal drag. *Tectonophysics*, *358*(1–4), 211–231. https://doi.org/10.1016/S0040-1951(02)00425-0

Bartholomaus, T., & Catania, G. (2013). Physical controls on ocean-terminating glacier variability in central west Greenland [Dataset]. *International Federation of Digital Seismograph Networks*. https://doi.org/10.7914/SN/YM_2013

Bina, C. R., & Helffrich, G. (1994). Phase transition Clapeyron slopes and transition zone seismic discontinuity topography. *Journal of Geophysical Research*, *99*(B8), 15853–15860. https://doi.org/10.1029/94JB00462

Brozena, J. M. (1995). *Kinematic GPS and aerogeophysical measurement: Gravity, topography and magnetics*. University of Cambridge.

Buiter, S. J. H., & Torsvik, T. H. (2014). A review of Wilson cycle plate margins: A role for mantle plumes in continental break-up along sutures? *Gondwana Research*, *26*(2), 627–653. https://doi.org/10.1016/j.gr.2014.02.007

Celli, N. L., Lebedev, S., Schaeffer, A. J., & Gaina, C. (2021). The tilted Iceland Plume and its effect on the North Atlantic evolution and magmatism. *Earth and Planetary Science Letters*, *569*, 117048. https://doi.org/10.1016/j.epsl.2021.117048

Chalmers, J. A. (1991). New evidence on the structure of the Labrador Sea/Greenland continental margin. *Journal of the Geological Society*, *148*(5), 899–908. https://doi.org/10.1144/gsjgs.148.5.0899

Cox, A. H. R. B. (1986). *Plate tectonics: How it works*. Blackwell Scientific Publications.

Cox, R. T. (1999). Hawaiian volcanic propagation and Hawaiian swell asymmetry: Evidence of northwestward flow of the deep upper mantle. *Tectonophysics*, *310*(1–4), 69–79. https://doi.org/10.1016/S0040-1951(99)00151-1

Darbyshire, F. A., Dahl-Jensen, T., Larsen, T. B., Voss, P. H., & Joyal, G. (2018). Crust and uppermost-mantle structure of Greenland and the Northwest Atlantic from Rayleigh wave group velocity tomography. *Geophysical Journal International*, *212*(3), 1546–1569. https://doi.org/10.1093/gji/ggx479

Deuss, A. (2007). Seismic observations of transition-zone discontinuities beneath hotspot locations. In *Special paper 430: Plates, plumes and planetary processes* (pp. 121–136). Geological Society of America. https://doi.org/10.1130/2007.2430(07)

Doubrovine, P. V., Steinberger, B., & Torsvik, T. H. (2012). Absolute plate motions in a reference frame defined by moving hot spots in the Pacific, Atlantic, and Indian oceans. *Journal of Geophysical Research*, *117*(B9), B09101. https://doi.org/10.1029/2011JB009072

Faccenda, M., & Dal Zilio, L. (2017). The role of solid–solid phase transitions in mantle convection. *Lithos*, *268*, 198–224. https://doi.org/10.1016/j.lithos.2016.11.007

Fahnestock, M., & Truffer, M. (2007). Understanding the current thinning and acceleration of the Jakobshavns Isbrae, Greenland [Dataset]. *International Federation of Digital Seismograph Networks*. https://doi.org/10.7914/SN/X3_2007

Forsyth, D. A., Morel-A-L'Huissier, P., Asudeh, I., & Green, A. G. (1986). Alpha Ridge and Iceland-products of the same plume? *Journal of Geodynamics*, *6*(1–4), 197–214. https://doi.org/10.1016/0264-3707(86)90039-6

Gao, S. S., & Liu, K. H. (2014a). Imaging mantle discontinuities using multiply-reflected P-to-S conversions. *Earth and Planetary Science Letters*, *402*, 99–106. https://doi.org/10.1016/j.epsl.2013.08.025

Gao, S. S., & Liu, K. H. (2014b). Mantle transition zone discontinuities beneath the contiguous United States. *Journal of Geophysical Research: Solid Earth*, *119*(8), 6452–6468. https://doi.org/10.1002/2014JB011253

Geist, D., & Richards, M. (1993). Origin of the Columbia Plateau and snake river plain: Deflection of the Yellowstone plume. *Geology*, *21*(9), 789. https://doi.org/10.1130/0091-7613(1993)021<0789:OOTCPA>2.3.CO;2

Goes, S., Yu, C., Ballmer, M. D., Yan, J., & van der Hilst, R. D. (2022). Compositional heterogeneity in the mantle transition zone. *Nature Reviews Earth and Environment*, *3*(8), 533–550. https://doi.org/10.1038/s43017-022-00312-w

Grocott, J., & McCaffrey, K. J. W. (2017). Basin evolution and destruction in an early proterozoic continental margin: The Rinkian fold–thrust belt of central west Greenland. *Journal of the Geological Society*, *174*(3), 453–467. https://doi.org/10.1144/jgs2016-109

Gu, Y. J., & Dziewonski, A. M. (2002). Global variability of transition zone thickness. *Journal of Geophysical Research*, *107*(B7), 2135. https://doi.org/10.1029/2001JB000489

Gu, Y. J., Dziewonski, A. M., & Agee, C. B. (1998). Global de-correlation of the topography of transition zone discontinuities. *Earth and Planetary Science Letters*, *157*(1–2), 57–67. https://doi.org/10.1016/S0012-821X(98)00027-2

Hanan, B. B., & Schilling, J.-G. (1997). The dynamic evolution of the Iceland mantle plume: The lead isotope perspective. *Earth and Planetary Science Letters*, *151*(1–2), 43–60. https://doi.org/10.1016/S0012-821X(97)00105-2

Hansen, S. E., & Nyblade, A. A. (2013). The deep seismic structure of the Ethiopia/Afar hotspot and the African superplume. *Geophysical Journal International*, *194*(1), 118–124. https://doi.org/10.1093/gji/ggt116

Hansen, S. E., Nyblade, A. A., & Benoit, M. H. (2012). Mantle structure beneath Africa and Arabia from adaptively parameterized P-wave tomography: Implications for the origin of Cenozoic Afro-Arabian tectonism. *Earth and Planetary Science Letters*, *319*(320), 23–34. https://doi.org/10.1016/j.epsl.2011.12.023

Holland, D. (2012). Observation of a glacier calving event using a network of GPS and Seismic sensors [Dataset]. *International Federation of Digital Seismograph Networks*. https://doi.org/10.7914/SN/YF_2012

Ishii, T., Kojitani, H., & Akaogi, M. (2018). Phase relations and mineral chemistry in pyrolitic mantle at 1600–2200°C under pressures up to the uppermost lower mantle: Phase transitions around the 660-km discontinuity and dynamics of upwelling hot plumes. *Physics of the Earth and Planetary Interiors*, *274*, 127–137. https://doi.org/10.1016/j.pepi.2017.10.005

Jenkins, J., Cottaar, S., White, R. S., & Deuss, A. (2016). Depressed mantle discontinuities beneath Iceland: Evidence of a garnet controlled 660 km discontinuity? *Earth and Planetary Science Letters*, *433*, 159–168. https://doi.org/10.1016/j.epsl.2015.10.053

Katsura, T. (2022). A revised adiabatic temperature profile for the mantle. *Journal of Geophysical Research: Solid Earth*, *127*(2), e2021JB023562. https://doi.org/10.1029/2021JB023562

Kerr, R. C., & Mériaux, C. (2004). Structure and dynamics of sheared mantle plumes. *Geochemistry, Geophysics, Geosystems*, *5*(12), Q12009. https://doi.org/10.1029/2004GC000749

Koppers, A. A. P., Becker, T. W., Jackson, M. G., Konrad, K., Müller, R. D., Romanowicz, B., et al. (2021). Mantle plumes and their role in Earth processes. *Nature Reviews Earth and Environment*, *2*(6), 382–401. https://doi.org/10.1038/s43017-021-00168-6

Kraft, H. A., Vinnik, L., & Thybo, H. (2018). Mantle transition zone beneath central-eastern Greenland: Possible evidence for a deep tectosphere from receiver functions. *Tectonophysics*, *728–729*, 34–40. https://doi.org/10.1016/j.tecto.2018.02.008

Kumar, P., Kind, R., Hanka, W., Wylegalla, K., Reigber, C., Yuan, X., et al. (2005). The lithosphere-asthenosphere boundary in the North-West Atlantic region. *Earth and Planetary Science Letters*, *236*(1–2), 249–257. https://doi.org/10.1016/j.epsl.2005.05.029

Lebedev, S., Schaeffer, A. J., Fullea, J., & Pease, V. (2018). Seismic tomography of the Arctic region: Inferences for the thermal structure and evolution of the lithosphere. *Geological Society, London, Special Publications*, *460*(1), 419–440. https://doi.org/10.1144/SP460.10

Lee, W. S., & Park, Y. (2013). Korea polar observation network [Dataset]. *International Federation of Digital Seismograph Networks*. https://doi.org/10.7914/SN/KP

Liu, H., Wang, W., Jia, X., Leng, W., Wu, Z., & Sun, D. (2018). The combined effects of post-spinel and post-garnet phase transitions on mantle plume dynamics. *Earth and Planetary Science Letters*, *496*, 80–88. https://doi.org/10.1016/j.epsl.2018.05.031

Lu, C., Grand, S. P., Lai, H., & Garnero, E. J. (2019). TX2019slab: A new P and S tomography model incorporating subducting slabs. *Journal of Geophysical Research: Solid Earth*, *124*(11), 11549–11567. https://doi.org/10.1029/2019JB017448

Martos, Y. M., Jordan, T. A., Catalán, M., Jordan, T. M., Bamber, J. L., & Vaughan, D. G. (2018). Geothermal heat flux reveals the Iceland hotspot track underneath Greenland. *Geophysical Research Letters*, *45*(16), 8214–8222. https://doi.org/10.1029/2018GL078289

Mériaux, C. A., Mériaux, A.-S., Schellart, W. P., Duarte, J. C., Duarte, S. S., & Chen, Z. (2016). Mantle plumes in the vicinity of subduction zones. *Earth and Planetary Science Letters*, *454*, 166–177. https://doi.org/10.1016/j.epsl.2016.09.001

Minakov, A., & Gaina, C. (2021). Probabilistic linear inversion of satellite gravity gradient data applied to the Northeast Atlantic. *Journal of Geophysical Research: Solid Earth*, *126*(12), e2021JB021854. https://doi.org/10.1029/2021JB021854

Mordret, A. (2018). Uncovering the Iceland hot spot track beneath Greenland. *Journal of Geophysical Research: Solid Earth*, *123*(6), 4922–4941. https://doi.org/10.1029/2017JB015104

Morgan, W. J. (1983). Hotspot tracks and the early rifting of the Atlantic (pp. 123–139). https://doi.org/10.1016/B978-0-444-42198-2.50015-8

Motyka, R., Fahnestock, M., & Truffer, M. (2010). Ice-ocean interaction at Nuuk tidewater glaciers [Dataset]. *International Federation of Digital Seismograph Networks*. https://doi.org/10.7914/SN/9D_2010

Moucha, R., & Forte, A. M. (2011). Changes in African topography driven by mantle convection. *Nature Geoscience*, *4*(10), 707–712. https://doi.org/10.1038/ngeo1235

Müller, R. D., Royer, J.-Y., & Lawver, L. A. (1993). Revised plate motions relative to the hotspots from combined Atlantic and Indian Ocean hotspot tracks. *Geology*, *21*(3), 275. https://doi.org/10.1130/0091-7613(1993)021<0275:RPMRTT>2.3.CO;2

Nelson, P. L., & Grand, S. P. (2018). Lower-mantle plume beneath the Yellowstone hotspot revealed by core waves. *Nature Geoscience*, *11*(4), 280–284. https://doi.org/10.1038/s41561-018-0075-y

Nettles, M. (2014). Understanding precambrian to present assembly of Greenland [Dataset]. *International Federation of Digital Seismograph Networks*. https://doi.org/10.7914/SN/XF_2014

O'Neill, C., Müller, D., & Steinberger, B. (2005). On the uncertainties in hot spot reconstructions and the significance of moving hot spot reference frames. *Geochemistry, Geophysics, Geosystems*, *6*(4), Q04003. https://doi.org/10.1029/2004GC000784

Peace, A. L., Foulger, G. R., Schiffer, C., & McCaffrey, K. J. W. (2017). Evolution of Labrador Sea-Baffin Bay: Plate or plume processes? *Geoscience Canada*, *44*(3), 91–102. https://doi.org/10.12789/geocanj.2017.44.120

Pourpoint, M., Anandakrishnan, S., Ammon, C. J., & Alley, R. B. (2018). Lithospheric structure of Greenland from ambient noise and earthquake surface wave tomography. *Journal of Geophysical Research: Solid Earth*, *123*(9), 7850–7876. https://doi.org/10.1029/2018JB015490

Rasmussen, M. B., Halldórsson, S. A., Gibson, S. A., & Guðfinnsson, G. H. (2020). Olivine chemistry reveals compositional source heterogeneities within a tilted mantle plume beneath Iceland. *Earth and Planetary Science Letters*, *531*, 116008. https://doi.org/10.1016/j.epsl.2019.116008

Rickers, F., Fichtner, A., & Trampert, J. (2013). The Iceland-Jan Mayen plume system and its impact on mantle dynamics in the North Atlantic region: Evidence from full-waveform inversion. *Earth and Planetary Science Letters*, *367*, 39–51. https://doi.org/10.1016/j.epsl.2013.02.022

Roest, W. R., & Srivastava, S. P. (1989). Seafloor spreading in the Labrador Sea: A new reconstruction. *Geology*, *17*(11), 1000. https://doi.org/10.1130/0091-7613(1989)017<1000:SFSITL>2.3.CO;2

Rogozhina, I., Petrunin, A. G., Vaughan, A. P. M., Steinberger, B., Johnson, J. V., Kaban, M. K., et al. (2016). Melting at the base of the Greenland ice sheet explained by Iceland hotspot history. *Nature Geoscience*, *9*(5), 366–369. https://doi.org/10.1038/ngeo2689

Shen, Y., Solomon, S. C., Bjarnason, I. T., Nolet, G., Morgan, W. J., Allen, R. M., et al. (2002). Seismic evidence for a tilted mantle plume and north–south mantle flow beneath Iceland. *Earth and Planetary Science Letters*, *197*(3–4), 261–272. https://doi.org/10.1016/S0012-821X(02)00494-6

Shervais, J. W., & Hanan, B. B. (2008). Lithospheric topography, tilted plumes, and the track of the Snake River–Yellowstone hot spot. *Tectonics*, *27*(5), TC5004. https://doi.org/10.1029/2007TC002181

Sleep, N. H. (1997). Lateral flow and ponding of starting plume material. *Journal of Geophysical Research*, *102*(B5), 10001–10012. https://doi.org/10.1029/97JB00551

Sleep, N. H., Ebinger, C. J., & Kendall, J.-M. (2002). Deflection of mantle plume material by cratonic keels. *Geological Society, London, Special Publications*, *199*(1), 135–150. https://doi.org/10.1144/GSL.SP.2002.199.01.08

Steinberger, B., Bredow, E., Lebedev, S., Schaeffer, A., & Torsvik, T. H. (2019). Widespread volcanism in the Greenland–North Atlantic region explained by the Iceland plume. *Nature Geoscience*, *12*(1), 61–68. https://doi.org/10.1038/s41561-018-0251-0

Steinberger, B., Sutherland, R., & O'Connell, R. J. (2004). Prediction of Emperor-Hawaii seamount locations from a revised model of global plate motion and mantle flow. *Nature*, *430*(6996), 167–173. https://doi.org/10.1038/nature02660

Tauzin, B., Debayle, E., & Wittlinger, G. (2008). The mantle transition zone as seen by global *Pds* phases: No clear evidence for a thin transition zone beneath hotspots. *Journal of Geophysical Research*, *113*(8), B08309. https://doi.org/10.1029/2007JB005364

Toyokuni, G., Matsuno, T., & Zhao, D. (2020). P wave tomography beneath Greenland and surrounding regions: 1. Crust and upper mantle. *Journal of Geophysical Research: Solid Earth*, *125*(12), e2020JB019837. https://doi.org/10.1029/2020JB019837

Toyokuni, G., & Zhao, D. (2021). P-wave tomography for 3-D radial and azimuthal anisotropy beneath Greenland and surrounding regions. *Earth and Space Science*, *8*(12), e2021EA001800. https://doi.org/10.1029/2021EA001800

Wessel, P., Luis, J. F., Uieda, L., Scharroo, R., Wobbe, F., Smith, W. H. F., & Tian, D. (2019). The Generic Mapping Tools version 6 [Software]. *Geochemistry, Geophysics, Geosystems*, *20*(11), 5556–5564. https://doi.org/10.1029/2019GC008515

Whitehead, J. A. (1982). Instabilities of fluid conduits in a flowing earth—Are plates lubricated by the asthenosphere? *Geophysical Journal International*, *70*(2), 415–433. https://doi.org/10.1111/j.1365-246X.1982.tb04975.x

Wilkinson, C. M., Ganerød, M., Hendriks, B. W. H., & Eide, E. A. (2017). Compilation and appraisal of geochronological data from the North Atlantic igneous province (NAIP). *Geological Society, London, Special Publications*, *447*(1), 69–103. https://doi.org/10.1144/SP447.10

Wölbern, I., Jacob, A. W. B., Blake, T. A., Kind, R., Li, X., Yuan, X., et al. (2006). Deep origin of the Hawaiian tilted plume conduit derived from receiver functions. *Geophysical Journal International*, *166*(2), 767–781. https://doi.org/10.1111/j.1365-246X.2006.03036.x

References From the Supporting Information

Kong, F., Gao, S. S., Liu, K. H., Ding, W., & Li, J. (2020). Slab dehydration and mantle upwelling in the vicinity of the Sumatra subduction zone: Evidence from receiver function imaging of mantle transition zone discontinuities. *Journal of Geophysical Research: Solid Earth*, *125*(9), e2020JB019381. https://doi.org/10.1029/2020JB019381

Liu, K. H., Gao, S. S., Silver, P. G., & Zhang, Y. (2003). Mantle layering across central South America. *Journal of Geophysical Research*, *108*(B11), 2510. https://doi.org/10.1029/2002JB002208